


Direct Comparison of Thermoelectric Devices Using Impedance Spectroscopy

CHUNG-YUL YOO ^{1,2}, HANA YOON,¹ and SANG HYUN PARK^{1,3}

1.—Separation and Conversion Materials Laboratory, Korea Institute of Energy Research, 152 Gajeong-ro, Yuseong-gu, Daejeon 34129, Republic of Korea. 2.—e-mail: cyoo@kier.re.kr. 3.—e-mail: parksh@kier.re.kr

The thermoelectric properties of devices based on bismuth telluride, skutterudite, and calcium manganese oxide have been investigated and compared using impedance spectroscopy at 23°C. Prior to the detailed analysis, Kramers–Kronig transformation tests were performed to examine the validity of the obtained impedance spectra. All the spectra were Kramers–Kronig transformable, and were interpreted using equivalent circuit fitting. The three key parameters (Seebeck coefficient, thermal conductivity, and electrical conductivity) and dimensionless figure of merit of bismuth telluride and skutterudite-based devices were successfully extracted from their respective impedance spectra. However, the thermal conductivity of the calcium manganese oxide-based device was overestimated, while the Seebeck coefficient and electrical conductivity values were reasonably accurate owing to their negligible thermoelectric effect at 23°C. We further proposed that the thermoelectric capacitance obtained from the impedance spectra could be a quantitative measure of the “propensity” of thermoelectric devices to generate thermoelectric power under an external temperature gradient.

Key words: Thermoelectric device, impedance spectroscopy, Kramers–Kronig transformation, thermoelectric properties

INTRODUCTION

Thermoelectric devices represent a promising technology for direct conversion of thermal energy to electrical energy from waste heat.¹ Significant research effort has been devoted to the fabrication and optimization of thermoelectric devices^{2–9} together with the development of highly efficient thermoelectric compositions^{10–13} to improve their thermoelectric conversion efficiency. However, most of these researches were aimed at investigating the resistive behavior of thermoelectric devices,^{2–9} while the capacitive behavior of the devices are less understood due to the lack of suitable measurement techniques.

Harman’s method¹⁴ and pulse-response techniques^{15,16} have been widely employed for both thermoelectric materials and devices to investigate their figure of merit and thermal diffusivity, respectively. However, additional measurements are still required for the assessment of their Seebeck coefficient, electrical conductivity, and heat capacity. Recently, it has been demonstrated that the three key parameters (Seebeck coefficient, thermal conductivity, and electrical conductivity) and figure of merit of thermoelectric devices can be determined simultaneously using an alternating-current impedance spectroscopy protocol under ambient and practical operating temperatures.^{17–24} By analyzing both resistive and capacitive responses from the impedance spectra, the detailed properties of thermoelectric devices can be obtained after fabrication of devices. The fundamental properties of BiTe-based devices, such as their thermoelectric capacitance and the time constants of their metallic

contacts and thermoelectric legs, have also been investigated using impedance spectroscopy.^{17,19,23} With the exception of BiTe-based devices, however, a detailed and systematic understanding of the factors affecting the properties of thermoelectric devices is lacking.

This work focuses on ascertaining the properties of three kinds of thermoelectric devices, combining resistive and capacitive responses from impedance spectroscopy. Two commercial devices, based on bismuth telluride and calcium manganese oxide, and an in-house-fabricated skutterudite-based device were employed to obtain an unambiguous interpretation of the resistive and capacitive processes of the devices from impedance spectra to obtain the thermoelectric properties of the devices quantitatively and systematically. Thermoelectric devices, rather than individual thermoelectric legs, were used to ensure the reproducibility of impedance spectroscopy measurements and to eliminate difficulties associated with establishing electrical contacts.

EXPERIMENTAL

A bismuth telluride (BiTe)-based device (multi-purpose type) was purchased from KELK Ltd using 404 thermoelectric legs (of dimensions 0.4 cm × 0.2 cm × 0.136 cm) assembled with a Pb solder, Cu electrodes, and polyimide insulating sheets (thickness = 0.002 cm, $\lambda = 0.12 \text{ W m}^{-1} \text{ K}^{-1}$). A calcium manganese oxide (CMO)-based device (CMO-32-62S) was purchased from TECTEG MFR using 64 thermoelectric legs (of dimensions 0.34 cm × 0.34 cm × 0.75 cm) assembled with Ag electrodes, an alumina insulating plate for the hot-side (thickness = 0.08 cm, $\lambda = 30 \text{ W m}^{-1} \text{ K}^{-1}$), and a cool gel pad for the cold-side (thickness = 0.06 cm, $\lambda = 10 \text{ W m}^{-1} \text{ K}^{-1}$). A two-couple skutterudite (SKD) device was prepared in our laboratory. Ti-metallized SKD pellets, with Ti/SKD/Ti structure, were prepared by spark plasma sintering (SPS-211LX, Fuji Electronic Industrial Co., Ltd.). Ti/SKD/Ti joints were cut into dimensions of 0.4 cm × 0.4 cm × 0.4 cm, then integrated to Cu electrodes on Al₂O₃ substrate (thickness of 0.076 cm, $\lambda = 19.6 \text{ W m}^{-1} \text{ K}^{-1}$) using Incusil-series brazing alloy on both sides. The fabrication process for Ti-metallized SKD device is similar to that for a FeNi-metallized SKD device, as described in detail in a previous report from our group.⁷

The thermoelectric devices were suspended in a vacuum chamber (0.1 kPa) to perform impedance spectroscopy measurements using an Autolab (PGSTAT302 N, Metrohm) with a 10 A booster as functions of frequency under open-circuit voltage conditions at 23°C. Measurements were performed by applying a sine-wave perturbation of 10 mV voltage amplitude in potentiostatic mode for BiTe-based devices, as optimized in our previous paper,¹⁹ and 1.66 A and 1.48 A optimum current amplitude

in galvanostatic mode for SKD- and CMO-based devices, respectively. Details of the optimum current amplitude of SKD- and CMO-based devices are given in the Results and Discussion. The resistance of the wires in the thermoelectric devices to establish electrical connections between the device and Autolab is less than 30 $\mu\Omega$; hence, the heat leakage from the wiring is negligible for the impedance spectroscopy measurements. The obtained impedance spectra were analyzed by fitting with the equivalent circuit model of $R_{\text{ohm}}(W_{\text{O}}W_{\text{S}})$, where W_{s} and W_{o} are the short and open Warburg elements, respectively, as follows¹⁹:

$$\begin{aligned} Z_{W_{\text{s}}}(j\omega) &= WR_{\text{s}}(j\omega WT_{\text{s}})^{-0.5} \tanh\left[(j\omega WT_{\text{s}})^{0.5}\right] \quad \text{and} \\ Z_{W_{\text{o}}}(j\omega) &= WR_{\text{o}}(j\omega WT_{\text{o}})^{-0.5} \coth\left[(j\omega WT_{\text{o}})^{0.5}\right]. \end{aligned} \quad (1)$$

The ohmic resistance (R_{ohm}), Warburg resistances (WR_{s} and WR_{o}), and time constants (WT_{s} and WT_{o}) can be determined using ZView software (Scribner Associates, Inc.). Satisfactory fitting results can be obtained for all impedance data ($\chi^2 < 4 \times 10^{-6}$). The electrical conductivity (σ), Seebeck coefficient (S), thermal conductivity (λ_{TEL}), and figure of merit (ZT) values can be calculated by using the following expressions:

$$\begin{aligned} R_{\text{ohm}} &= n \frac{L}{\sigma A}, \quad WR_{\text{o}} = \frac{2nS^2 TL_{\text{C}}}{\lambda_{\text{C}} A}, \\ WR_{\text{s}} &= \frac{nS^2 TL}{\lambda_{\text{TEL}} A}, \quad \text{and } ZT = \frac{S^2 \sigma}{\lambda_{\text{TEL}}} T, \end{aligned} \quad (2)$$

where TEL and C correspond to the thermoelectric leg and contact, including both the metallic contact and insulating sheet. n is the number of thermoelectric legs, S is the averaged Seebeck coefficient for both p - and n -type thermoelectric legs, T is the absolute temperature, A is the area of a single thermoelectric leg, L is the length of a single thermoelectric leg, and λ_{C} is equivalent to the thermal conductivity of the insulating plates.

RESULTS AND DISCUSSION

The current amplitude values used for impedance spectroscopy of the SKD- and CMO-based devices were optimized by employing the Peltier power density ($STI_{\text{OSC}}/A_{\text{t}}$) in accordance with the results of Beltrán-Pitarch et al.,²⁰ where S is the averaged Seebeck coefficient for both p - and n -type thermoelectric legs, T is the absolute temperature, I_{OSC} is the oscillation current amplitude, and A_{t} is the total area of thermoelectric legs integrated in the device. We performed impedance spectroscopy measurements as a function of oscillation current amplitude for both SKD- and CMO-based devices, and then performed equivalent circuit fitting to extract the Seebeck coefficient values. These Seebeck coefficients were

compared with the average Seebeck coefficient for both *p*- and *n*-type thermoelectric legs. As shown in Fig. S1 in the Electronic Supplementary Material, the Seebeck coefficient values of impedance spectra with an oscillation current amplitude of 1.66 A (Peltier power density corresponding to 1000 W m^{-2}) for SKD-based devices and 1.48 A (Peltier power density corresponding to 150 W m^{-2}) for CMO-based devices exhibit the best agreement with the average Seebeck coefficient for both *p*- and *n*-type thermoelectric legs, and no significant variation in the ohmic and thermoelectric resistances is caused by the Joule heating. We have characterized both SKD- and CMO-based devices using the above optimum current amplitudes.

Prior to the equivalent circuit analysis to obtain the relevant parameters describing thermoelectric properties, Kramers–Kronig (KK) transformation tests were performed to validate the measured impedance data of thermoelectric devices. The results of these tests provide the relationship between the real and imaginary parts of the impedance spectra and reconstructs the real part of the impedance spectrum to its imaginary part and vice versa from 0 to ∞ in the frequency domain, as follows^{25,26}:

$$\begin{aligned} Z_{\text{im, KK}}(\omega) &= \frac{2\omega}{\pi} \int_0^{\infty} \frac{Z_{\text{re}}(x) - Z_{\text{re}}(\omega)}{x^2 - \omega^2} dx \\ Z_{\text{re, KK}}(\omega) &= R_{\infty} + \frac{2}{\pi} \int_0^{\infty} \frac{xZ_{\text{im}}(x) - \omega Z_{\text{im}}(\omega)}{x^2 - \omega^2} dx \end{aligned} \quad (3)$$

where $R(\infty) = Z_{\text{re}}(\infty)$. This interdependent KK relation can be valid only under the assumption that the measured response arises solely due to the applied voltage/current perturbation. The system remains in steady state over time (equilibrated to the measurement condition). In addition, no initial parameters are required for the KK test. Thus, the KK test is a very effective evaluation to exclude impedance data containing non-steady-state behavior. Before detailed analysis of impedance spectra, the KK test is used to yield the residual plot from the differences, $\Delta Z_{\text{re}}(\omega)$ and $\Delta Z_{\text{im}}(\omega)$, between the measured data (Z_{re} and Z_{im}) and KK transformation results ($Z_{\text{re, KK}}$ and $Z_{\text{im, KK}}$) as a function of frequency:

$$\begin{aligned} \Delta Z_{\text{re}}(\omega) &= \frac{(Z_{\text{re}}(\omega) - Z_{\text{re, KK}}(\omega))}{|Z_{\text{KK}}|} \quad \text{and} \\ \Delta Z_{\text{im}}(\omega) &= \frac{(Z_{\text{im}}(\omega) - Z_{\text{im, KK}}(\omega))}{|Z_{\text{KK}}|}. \end{aligned} \quad (4)$$

Figure 1 shows a set of KK test results from the impedance spectra corresponding to devices based on BiTe, SKD, and CMO. All the impedance spectra were KK transformable, only showing a randomly distributed noise along the frequency axis with

residual errors and goodness of fitness (χ^2) below 0.3% and 10^{-6} , respectively. The relatively large residuals observed for the SKD device were partly due to the small electrical resistance about two orders of magnitudes compared to those of other devices. Nevertheless, it has been reported that residuals smaller than 0.5% over the entire frequency range indicate a good-quality valid spectrum under the steady-state conditions, thus allowing complex nonlinear least-square analysis using an equivalent circuit.²⁷

Figure 2 shows the impedance spectra fitted using the equivalent circuit fitting of the thermoelectric devices at 23°C. As shown in Figure 2, the left intercept on the x-axis in the high-frequency region is due to the electrical resistance (R_{ohm}), while the dispersion along the y-axis from high to low frequency is due to the thermoelectric process of electrical contacts (WR_{O} and WT_{O}) and thermoelectric legs (WR_{s} and WT_{s}) of the device. The asymmetric dispersion of the impedance spectra (the deviation from Cole–Cole arcs) at high frequency is due to the thermal conductivity mismatch between metal electrodes, whereas the compressed arc at the real axis primarily comprises the response thermoelectric materials upon external voltage or current perturbation.^{17,20} The fitting parameters obtained using Eq. 2 and the calculated values of S , λ_{TEL} , σ , and ZT are summarized in Table I. The values of ZT of the thermoelectric devices were in the order BiTe > SKD > CMO-based device, reflecting the nature of the constituting thermoelectric leg materials. The operating hot-side temperature range for thermoelectric power generation by the BiTe, SKD, and CMO-based devices are 50–200°C, 300–600°C, and 400–800°C; thus, one could expect that the ZT at 23°C (cold-side temperature) is inversely proportional to the operating hot-side temperature of the device. The BiTe device in this study shows 3% higher ZT value (0.733) than that (0.720) obtained in ambient air due to the heat convection effect²²; however, the result obtained for the BiTe device is in good agreement with our previous report.¹⁹ The ZT (0.13) of the SKD-based device is 35% lower than that of the average value of *p*-type and *n*-type SKD materials (0.2).⁷ This is partly due to the $\sim 20\%$ increase in electrical resistivity and λ_{TEL} during device fabrication, while the values of S is similar to the average absolute magnitude for *p*- and *n*-type SKD materials ($\sim 133 \mu\text{V K}^{-1}$). The relatively large errors associated with the calculated S , λ_{TEL} , and ZT are due to the difficulty in determining the very low contact resistance ($WR_{\text{o}} \approx 100 \mu\Omega$) from the equivalent circuit fitting for the SKD-based device. However, the thermoelectric parameters, calculated from the analysis of a single impedance spectrum, shows reasonable agreement with the values of SKD materials.⁷ The CMO-based device has an asymmetric insulating plate structure, the average values of thickness and thermal conductivity (thickness = 0.07 cm, $\lambda = 20 \text{ W m}^{-1} \text{ K}^{-1}$) values of

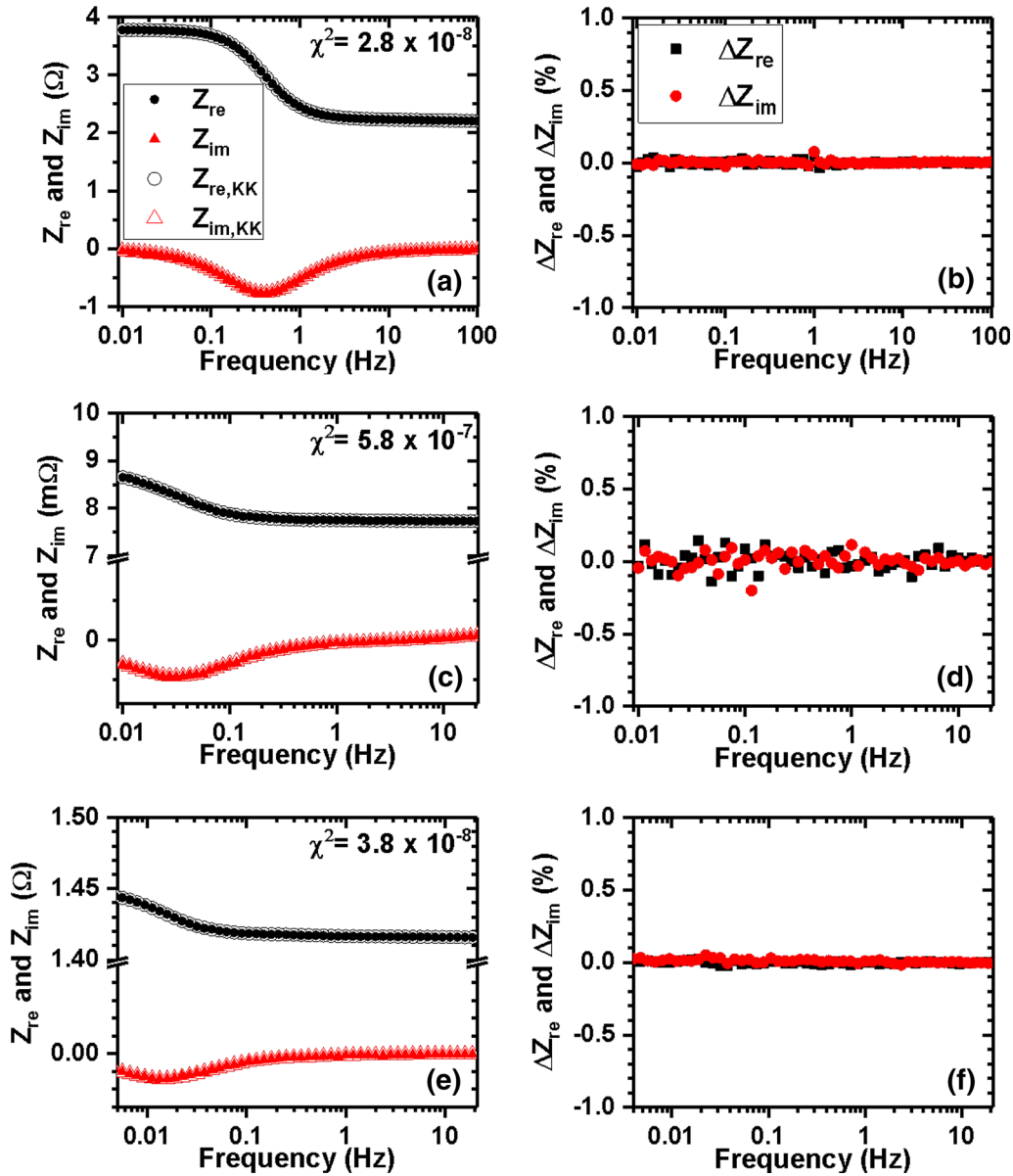


Fig. 1. Impedance spectroscopy data (filled symbol) and Kramers–Kronig transformation results (empty symbol) for devices based on (a) BiTe, (c) SKD, and (e) CMO and the residuals of Kramers–Kronig transformation results for devices based on (b) BiTe, (d) SKD, and (f) CMO.

which were used to obtain ZT and the three key parameters. The ZT value (0.023) of the CMO-based device is much lower than those of BiTe and SKD-based devices due to its negligible thermoelectric property at 23°C. The calculated λ_{TEL} ($36 \text{ W m}^{-1} \text{ K}^{-1}$) is about 12 times higher than those provided by the manufacturer and those reported in the literature ($\sim 3 \text{ W m}^{-1} \text{ K}^{-1}$),^{28,29} while the S ($310 \mu\text{V K}^{-1}$) and σ (293 S cm^{-1}) values of the CMO-based device are similar to the values obtained from the manufacturer ($\sim 225 \mu\text{V K}^{-1}$ and $\sim 200 \text{ S cm}^{-1}$, respectively). The λ_{TEL} value was over-estimated possibly due to the negligible thermoelectric effect of the CMO-based device, which, in turn, was due to its small ZT (< 0.1) at 23°C. Even though the operating hot-side

temperatures of the SKD and CMO-based devices are much higher than 23°C, the issue of the electrical and thermal contacts of the SKD and CMO-based devices can be assessed quickly by performing impedance spectroscopy measurements at 23°C. The high-temperature properties of the SKD and CMO-based devices will be further investigated in future studies.

Figure 3 shows the comparison of the power factors ($\sigma \cdot S^2$) and thermoelectric time constants (WT_s) of the BiTe-, SKD-, and CMO-based devices. The WT_s values were in the order of CMO > SKD > BiTe-based devices (the value of one device was 60-times higher than that of the one with the lower value), concomitant with the hot-side operating temperature of the device. However, the power

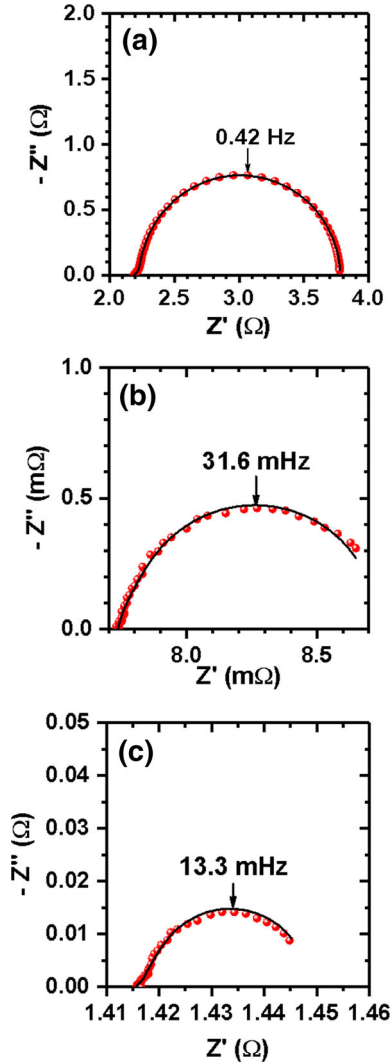


Fig. 2. Impedance spectra (filled symbol) and equivalent circuit fitting results (line) of the devices based on (a) BiTe, (b) SKD, and (c) CMO at 23°C and 0.1 kPa (the number denotes the frequency value of the top of the arc for each impedance spectrum).

factor varies only about two times between the devices in the same order as described above. This observation implied that the heat diffusion, from the hot side to cold side through the thermoelectric legs, was suppressed for the SKD and CMO-based devices operating under a larger temperature gradient than the BiTe-based device, which slightly increased the power factor. The time needed for heat diffusion across the thermoelectric legs is quantitatively determined by the thermoelectric time constant upon perturbation for the impedance spectroscopy measurements.^{18,19} During these measurements, the effective temperature profiles in the thermoelectric legs vary upon applying voltage/current perturbation, which produces variation in the Seebeck voltage. From the point of view of an external circuit, this behavior could be interpreted as the accumulation of electrical charge with a large capacitance, or the so-called “thermoelectric

capacitance.” For characterizing thermoelectric devices using impedance spectroscopy, thermoelectric capacitance could be a descriptor for converting the temperature gradient with frequency, caused by the external voltage/current perturbation in the form of electric current and Seebeck voltage. Thermoelectric capacitance (C_{TEL}) is defined as.^{17,19}

$$C_{\text{TEL}} = \frac{WT_s}{WR_s} = \frac{I}{S} \left(\frac{dT}{dt} \right)^{-1}, \quad (5)$$

where I is the electric current and S is the Seebeck coefficient. Since electrical capacitance is much smaller than thermal capacitance, the extremely large thermoelectric capacitances of the thermoelectric devices in this study signify that C_{TEL} is limited by the thermal capacitance, reflecting that the thermoelectric charge carriers and heat flow are highly correlated. Furthermore, C_{TEL} can be considered a measure of the “propensity” of a thermoelectric device to generate thermoelectric power under an external temperature gradient. Figure 3 shows the comparison of the volume-specific C_{TEL} of thermoelectric devices using the number and dimensions of thermoelectric legs to enable comparison between the devices. The volume-specific C_{TEL} varies by about six orders of magnitudes in the order SKD > CMO > BiTe-based device. The SKD-based device exhibits 30-times higher volume-specific C_{TEL} than a CMO-based device due to its small thermoelectric resistance (WR_s) (Table I). Since the Seebeck coefficients of all devices are between $100 \mu\text{V K}^{-1}$ and $300 \mu\text{V K}^{-1}$, the large variation in volume-specific C_{TEL} is mainly due to the difference in the thermoelectric current under temperature gradient. Therefore, C_{TEL} could provide a quantitative comparison guideline for the development and optimization of thermoelectric materials and devices.

CONCLUSIONS

In this study, we have investigated the thermoelectric properties of devices based on bismuth telluride, skutterudite, and calcium manganese oxide using impedance spectroscopy. Our key findings are as follows:

1. The impedance spectra of all the thermoelectric devices are Kramers–Kronig-transformable, showing only a randomly distributed noise. Kramers–Kronig-transformable impedance spectra enable complex nonlinear least square analysis using equivalent circuit to extract thermoelectric properties of the devices.
2. The obtained thermoelectric parameters of devices based on bismuth telluride and skutterudite are in good agreement with the values obtained from the manufacturer and those reported in the literature. The thermal conductivity of a calcium manganese oxide-based device shows a large discrepancy due to the

Table I. Summary of values (and associated errors) of equivalent circuit fitting and thermoelectric parameters of devices based on BiTe, SKD, and CMO

Device	Equivalent circuit fitting parameters		Three key thermoelectric parameters and figure of merit (ZT)	
	Parameter	Value	Parameter	Value
BiTe	$R_{ohm}(\Omega)$	2.18 ± 0.01	Seebeck coefficient ($S, \mu\text{V K}^{-1}$)	202 ± 4
	$WR_o(\Omega)$	0.206 ± 0.009	Thermal conductivity ($\lambda_{TEL}, \text{W m}^{-1} \text{K}^{-1}$)	0.53 ± 0.01
	$WR_S(\Omega)$	1.60 ± 0.01	Electrical conductivity ($\sigma, \text{S cm}^{-1}$)	315 ± 1
	$WT_o(\text{s})$	0.0335 ± 0.0018	ZT	0.73 ± 0.03
	$WT_S(\text{s})$	0.387 ± 0.02		
SKD	$R_{ohm}(\Omega)$	$7.72 \pm 0.01 \times 10^{-3}$	Seebeck coefficient ($S, \mu\text{V K}^{-1}$)	138 ± 21
	$WR_o(\Omega)$	$1.12 \pm 0.38 \times 10^{-4}$	Thermal conductivity ($\lambda_{TEL}, \text{W m}^{-1} \text{K}^{-1}$)	5.64 ± 1.12
	$WR_S(\Omega)$	$1.02 \pm 0.12 \times 10^{-3}$	Electrical conductivity ($\sigma, \text{S cm}^{-1}$)	1295 ± 2
	$WT_o(\text{s})$	0.215 ± 0.068	ZT	0.131 ± 0.15
	$WT_S(\text{s})$	8.30 ± 0.31		
CMO	$R_{ohm}(\Omega)$	1.416 ± 0.01	Seebeck coefficient ($S, \mu\text{V K}^{-1}$)	310 ± 12
	$WR_o(\Omega)$	0.011 ± 0.001	Thermal conductivity ($\lambda_{TEL}, \text{W m}^{-1} \text{K}^{-1}$)	36 ± 2
	$WR_S(\Omega)$	0.033 ± 0.001	Electrical conductivity ($\sigma, \text{S cm}^{-1}$)	293 ± 2
	$WT_o(\text{s})$	0.01 ± 0.001	ZT	0.023 ± 0.001
	$WT_S(\text{s})$	22.27 ± 0.68		

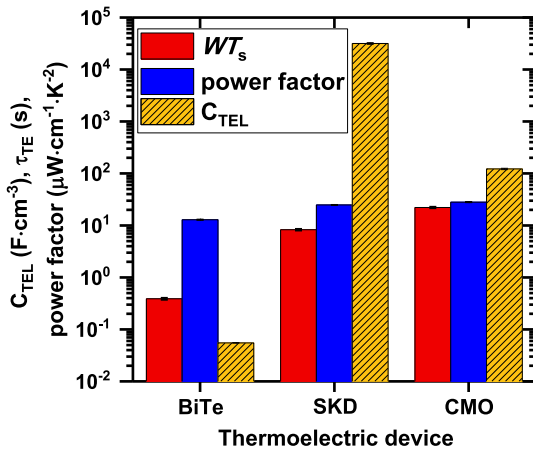


Fig. 3. Comparison of the power factor ($\sigma \cdot S^2$), thermoelectric time constant (WT_S), thermoelectric capacitance (C_{TEL}) (with error bars) for the BiTe, SKD, and CMO-based devices.

extremely low figure of merit at 23°C, while Seebeck coefficient and electrical conductivity values agree with the values obtained from the manufacturer.

- Thermoelectric capacitance can be utilized as a quantitative measure of the “propensity” of thermoelectric devices to generate thermoelectric power under an external temperature gradient.

ACKNOWLEDGMENTS

This work was supported by the Korea Institute of Energy Technology Evaluation and Planning (KETEP) and the Ministry of Trade, Industry & Energy (MOTIE) of the Republic of Korea (No.

20172010000830). This research was also supported by the National Research Foundation of Korea (NRF) Grant funded by the Korean Government (MSIP)(NRF-2015R1A5A1036133). Yeongseon Kim (Korea Advanced Institute of Science and Technology) and Juyeon Hwang (Chungnam National University) are gratefully acknowledged for preparation of the SKD-based device. Dr. Jorge Garcia-Cañadas (Universitat Jaume I) is gratefully acknowledged for fruitful discussions.

ELECTRONIC SUPPLEMENTARY MATERIAL

The online version of this article (<https://doi.org/10.1007/s11664-018-6777-5>) contains supplementary material, which is available to authorized users.

REFERENCES

- D.B. Gingerich and M.S. Mauter, *Environ. Sci. Technol.* 49, 8297 (2015).
- H. Wang, R. McCarty, J.R. Salvador, A. Yamamoto, and J. König, *J. Electron. Mater.* 43, 2274 (2014).
- G. Nie, S. Suzuki, T. Tomida, A. Sumiyoshi, T. Ochi, K. Mukaiyama, M. Kikuchi, J.Q. Guo, A. Yamamoto, and H. Obara, *J. Electron. Mater.* 46, 2640 (2017).
- D. Zhao, C. Tian, S. Tang, Y. Liu, L. Jiang, and L. Chen, *Mater. Sci. Semicond. Process.* 13, 221 (2010).
- J.Q. Guo, H.Y. Geng, T. Ochi, S. Suzuki, M. Kikuchi, Y. Yamaguchi, and S. Ito, *J. Electron. Mater.* 41, 1036 (2012).
- J.R. Salvador, J.Y. Cho, Z. Ye, J.E. Moczysgemba, A.J. Thompson, J.W. Sharp, J.D. Koenig, R. Maloney, T. Thompson, J. Sakamoto, H. Wang, and A.A. Wereszczak, *Phys. Chem. Chem. Phys.* 16, 12510 (2014).
- S.H. Park, Y. Jin, J. Cha, K. Hong, Y. Kim, H. Yoon, C.-Y. Yoo, and I. Chung, *ACS Appl. Energy Mater.* 1, 1603 (2018).

8. X. Hu, P. Jood, M. Ohta, M. Kunii, K. Nagase, H. Nishiata, M.G. Kanatzidis, and A. Yamamoto, *Energy Environ. Sci.* 9, 517 (2016).
9. K. Kato, Y. Hatasako, M. Kashiwagi, H. Hagino, C. Adachi, and K. Miyazaki, *J. Electron. Mater.* 43, 1733 (2014).
10. O. Appel, M. Schwall, D. Mogilyansky, M. Köhne, B. Balke, and Y. Gelbstein, *J. Electron. Mater.* 42, 1340 (2013).
11. O. Appel, T. Zilber, S. Kalabukhov, O. Beeri, and Y. Gelbstein, *J. Mater. Chem. C* 3, 11653 (2015).
12. B. Dado, Y. Gelbstein, D. Mogilansky, V. Ezersky, and M.P. Dariel, *J. Electron. Mater.* 39, 2165 (2010).
13. Y. Gelbstein, Z. Dashevsky, and M.P. Dariel, *Phys. Status Solidi Rapid Res. Lett.* 1, 232 (2007).
14. T.C. Harman, *J. Appl. Phys.* 29, 1373 (1958).
15. G.J. Snyder, J.-P. Fleurial, T. Caillat, R. Yang, and G. Chen, *J. Appl. Phys.* 92, 1564 (2002).
16. J.N. Mao, H.X. Chen, H. Jia, and X.L. Qian, *J. Appl. Phys.* 112, 014514 (2012).
17. J. García-Cañadas and G. Min, *J. Electron. Mater.* 43, 2411 (2014).
18. J. García-Cañadas and G. Min, *J. Appl. Phys.* 116, 174510 (2014).
19. C.-Y. Yoo, Y. Kim, J. Hwang, H. Yoon, B.J. Cho, G. Min, and S.H. Park, *Energy* 152, 834 (2018).
20. B. Beltrán-Pitarch, J. Prado-Gonjal, A.V. Powell, P. Ziolkowski, and J. García-Cañadas, *J. Appl. Phys.* 124, 25105 (2018).
21. B. Beltrán-Pitarch, L. Márquez-García, G. Min, and J. García-Cañadas, *Meas. Sci. Technol.* 28, 045902 (2017).
22. B. Beltrán-Pitarch and J. García-Cañadas, *J. Appl. Phys.* 123, 084505 (2018).
23. R. Mesalam, H.R. Williams, R.M. Ambrosi, J. García-Cañadas, and K. Stephenson, *Appl. Energy* 226, 1208 (2018).
24. M. Otsuka, Y. Hasegawa, T. Arisaka, R. Shinozaki, and H. Morita, *Appl. Phys. Express* 10, 115801 (2017).
25. B.A. Boukamp, *J. Electrochem. Soc.* 142, 1885 (1995).
26. B.A. Boukamp, *Solid State Ion.* 169, 65 (2004).
27. B. Hirschorn and M.E. Orazem, *J. Electrochem. Soc.* 156, C345 (2009).
28. Y. Zhou, I. Matsubara, R. Funahashi, G. Xu, and M. Shikano, *Mater. Res. Bull.* 38, 341 (2003).
29. J.W. Park, D.H. Kwak, S.H. Yoon, and S.C. Choi, *J. Alloys Compd.* 487, 550 (2009).